Urban Ecosyst (2011) 14:617–634
DOI 10.1007/s11252-011-0184-5

Nature of vegetation and building morphology characteristics across a city: Influence on shadow patterns and mean radiant temperatures in London

Fredrik Lindberg · C. S. B. Grimmond

Published online: 15 June 2011

Abstract Vegetation and building morphology characteristics are investigated at 19 sites on a north-south LiDAR transect across the megacity of London. Local maxima of mean building height and building plan area density at the city centre are evident. Surprisingly, the mean vegetation height (z_{v3}) is also found to be highest in the city centre. From the LiDAR data various morphological parameters are derived as well as shadow patterns. Continuous images of the effects of buildings and of buildings plus vegetationon sky view factor (ψ) are derived. A general reduction of ψ is found, indicating the importance of including vegetation when deriving ψ in urban areas. The contribution of vegetation to the shadowing at ground level is higher during summer than in autumn. Using these 3D data the influence on urban climate and mean radiant temperature (T_{mrt}) is calculated with SOLWEIG. The results from these simulations highlight that vegetation can be most effective at reducing heat stress within dense urban environments in summer. The daytime average T_{mrt} is found to be lowest in the densest urban environments due to shadowing; foremost from buildings but also from trees. It is clearly shown that this method could be used to quantify the influence of vegetation on T_{mrt} within the urban environment. The results presented in this paper highlight a number of possible climate sensitive planning practices for urban areas at the local scale (i.e. 10^2- 5×10^3 m).

Keywords LiDAR · Shadow patterns · Mean radiant temperature · Sky view factor · Urban vegetation · Urban morphology · SOLWEIG · Spatial variability · Urban trees

F. Lindberg · C. S. B. Grimmond
Environmental Monitoring and Modelling Group, Department of Geography, King's College London, The Strand, London WC2R 2LS, UK

F. Lindberg (✉)
Department of Earth Sciences, University of Gothenburg, Box 460, Gothenburg SE-405 30, Sweden
e-mail: fredrikl@gvc.gu.se

Introduction

Predictions of human-induced climate change suggest increases in surface air temperatures anywhere between 0.5 and 6.5°C over the next 100 years (IPCC 2007). In temperate climates, a 2–3°C increase in average summer air temperatures will double the frequency of periods characterized by extremely high air temperatures (WHO/WMO/UNEP 1996), which will result in more frequent, more intense and longer lasting episodes of heat waves (Meehl and Tebaldi 2004). It is also suggested that climate change could magnify the urban heat island effect in some locations (McCarthy et al. 2010). This calls for an improved understanding of how the variations of microclimates within an urban setting influence people's health and well-being. Of particular importance are human thermal comfort issues. During extreme heat waves, like those that occurred in central Europe in 2003, heat stress can have profound effects on people's health and well-being, with substantial economic consequences (Pascal et al. 2006). By taking climate issues into consideration in the urban planning process by, for example, increasing the amount of vegetation in urban areas, it is possible to create less stressful conditions and thus reduce the frequency of heat stroke and increase overall comfort during heat waves in cities (e.g. Matzarakis and Endler 2010).

The effect of vegetation on urban climate has been investigated for some time (e.g. Honjo and Takakura 1990–1991; Upmanis et al. 1998; Akbari et al. 2001). Urban green infrastructure can cool air by evapotranspiration (Grimmond and Oke 1991); shade parts of the ground and walls, which results in a reduction of the radiant and surface temperature (Ca et al. 1998; Simpson 2002); modify wind velocity and direction (Heisler 1990); absorb particulate matter that falls as air temperatures decrease in the evening; and filter dust and noise (e.g. Akbari 2002). Considering the influence of vegetation on thermal comfort, many studies deal with vegetation mitigation of heat stress in hot arid regions (e.g. Masmoudi and Mazouz 2004; Ali-Toudert and Mayer 2006, 2007b; Shashua-Bar et al. 2010) and in mid-latitude urban areas (e.g. Matzarakis et al. 1999; Picot 2004; Robitu et al. 2006; Ali-Toudert and Mayer 2007a; Lin et al. 2010). In general, these studies show that vegetation shadowing can have a large effect in reducing heat stress in urban areas. However, they typically consider only one point in space or a small area of interest such as a square or a street canyon.

Accurate and reliable spatial data of vegetation cover and in particular the 3D characteristics do not usually exist. Therefore, land cover data are often used to incorporate vegetation in various studies. However, Hirano et al. (2004) showed that small patches of vegetation such as street and garden trees, which in general are excluded from most land cover datasets, could have a significant impact on the climate in urban areas. Until recently, 3D structures and biodiversity have been restricted to local measurements or large scale generalizations whereas now Light Detecting And Ranging (LiDAR) and Radio Detecting And Ranging (RADAR) data are able to fill this gap (Bergen et al. 2009). Due to the complex geometry and diversity in the urban environment, high resolution datasets are preferable to extract reliable 3D vegetation information which makes airborne LiDAR a suitable data acquisition method. LiDAR provides height and structural information over large geographic areas in a time-efficient fashion and at relatively low cost. In urban environments LiDAR data are seen as a critical and innovative way to improve the characterization of both vegetation and building structures and attributes (Goodwin et al. 2009) while providing precise estimates of 3D properties of vegetation (e.g. Holmgren and Persson 2004; Næsset 2004). Using these data it is possible to differentiate between different tree species using intensity data (Kim et al. 2009) and to derive a 2.5D Digital Elevation Model (DEM) that includes buildings and vegetation to model solar flux and shadow patterns (Yu et al. 2009). However, treating vegetation as 2.5D objects, excluding

trunk zones (volume between the canopy and the ground) will cause errors (Chapman 2008). These errors can be removed by applying the shadow casting algorithm of Lindberg and Grimmond (2011).

This paper explores the nature of the spatial variations of various building and vegetation characteristics across an urban area. Using this vegetation and building morphology information, the influence of sky view factor, urban climate and mean radiant temperature (T_{mrt}), a variable used to estimate human thermal comfort, are investigated at the local scale. Unlike earlier studies that have focused on a small area within an urban setting, here a modelling approach is taken to investigate larger spatial domains in different areas within the megacity of London, UK. The **SO**lar and **L**ong**W**ave **E**nvironmental **I**rradiance **G**eometry (SOLWEIG) model (Lindberg et al. 2008) is used to estimate spatial and temporal effects of vegetation and urban morphology on daytime shadow patterns, radiative properties and thus T_{mrt}.

Methods

Study area and model domains

The study areas originate from a NERC ARSF (Natural Environment Research Council, Airborne Research & Survey Facility) north-south LiDAR flight transect through Greater London (51°30′N, 00°07′W) which consists of 33 Boroughs with 7.5 million people (Fig. 1). From that transect 19 (400-m x 400-m) sub-domains are extracted and used (Fig. 1). The whole transect is not examined due to the large amount of data points and hence long computation time. The spatial resolution on the ground is set to 2 m.

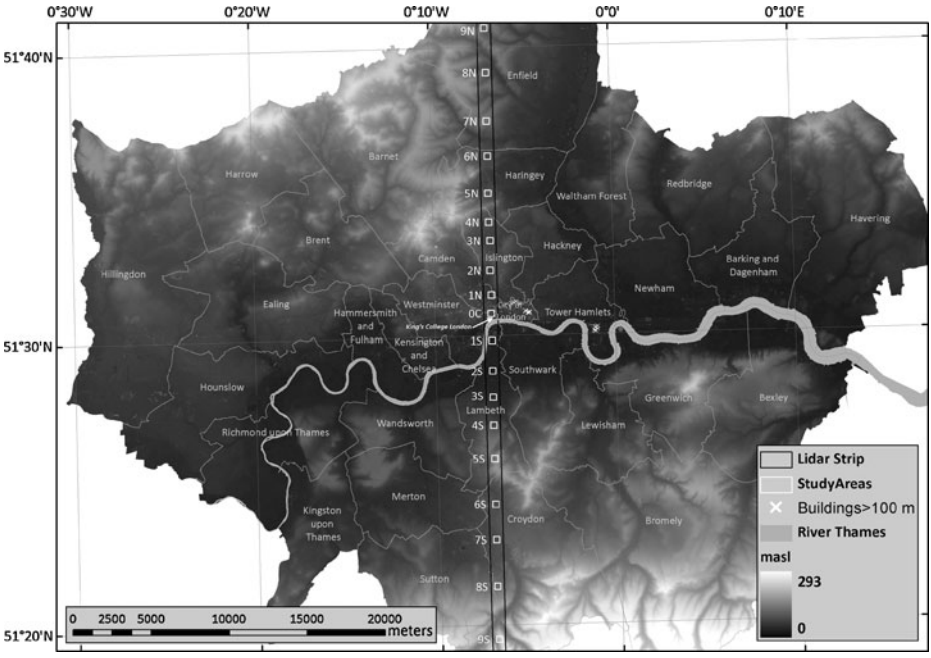

Fig. 1 Greater London (with 32 Boroughs and the City of London) showing LiDAR transect and the 19 study areas

LiDAR characteristics and data preprocessing

The spatial data were acquired on 14 August 2008 using an Optech ALTM 3033 LiDAR system, operating at a flight altitude of 900-m above ground level. The sensor was configured to record first and last returns as well as intensity values with a pulse frequency of 33 kHz using a maximum off-nadir view angle of 20° and a wavelength of 1064 nm. The beam-divergence was set to 0.21 mrads. The area surveyed includes an approximately 0.65-km × 50-km north to south transect passing over the central parts of London and a single flight line was used. The average point density on the ground was 0.71 m^{-2}. The 19 study areas were located centrally within the transect to exclude large off-nadir angles since the laser beam moves across the track resulting in a Z-shaped pattern with lower density distributed points at the edge of the field of view. If a pulse included a single and last return within a height interval of 0.3 m, one pulse was categorized as a single pulse return.

To derive the data, several steps and software systems were used. Most of the GIS preprocessing was done in ESRI's ArcInfo 9.3 and all filtering procedures presented used MathWorks MATLAB®. For SOLWEIG 2.0 the input spatial datasets required are (Lindberg and Grimmond 2011): a ground and building Digital Elevation Model (DEM), a vegetation canopy DEM and a trunk zone DEM. First the LiDAR points within each study area were extracted using FUSION/LDV (version 2.70- McGaughey 2009) from the main LiDAR cloud (46399632 points) (Fig. 2a). The GroundFilter algorithm within FUSION/LDV was used to identify those last and single returns that correspond to probable bare-earth surface points. These points were gridded to create a bare-earth DEM (Fig. 2b). To separate points located on building roofs, building footprints extracted from the OS MasterMap® Topography Layer (Ordnance Survey 2010) land use dataset were used. First and single returns outside the building footprints were stored separately to be used as 'potential' vegetation points. By combining the building points dataset and the bare-earth DEM, a ground and building DEM was created (Fig. 2c) (hereafter referred to as building DEM).

Height attributes for each vegetation pixel were compared with the bare-earth DEM and those lower than 2.5-m above ground were removed from the dataset. After points below 2.5-m agl were removed, urban features such as building walls, power lines, masts etc. were still present and had to be removed in order to generate a vegetation canopy DEM (Fig. 2d). To remove these non-vegetation features a similar filtering approach to Goodwin et al. (2009) was used. The first filter applied removed the linear features in the dataset. A 9×9 pixels moving window was used for a series of lines oriented 0° to 179°. When the number of pixels including vegetation points that intercepts a projected line was >4 points of the possible 9 and less than 3 of the surrounding pixels in the window were classified as vegetation, the vegetation pixels were removed. A second filter was applied to fill gaps caused by the sampling patterns of LiDAR and inconsistent detection of vegetation points. This was a 3×3 pixel moving kernel that classified a pixel as vegetation if six or more of the surrounding eight pixels were classified as vegetation (Goodwin et al. 2009). A final 3×3 pixel kernel filter was applied to remove single pixels classified as vegetation when none of the surrounding 8 pixels were non-vegetation pixels (e.g. masts, lamp posts etc). Remaining vegetation pixels were used to generate the canopy DEM with a height value or non-tree pixels assigned 0-m (Fig. 2e).

Vegetation has small gaps that allow laser light to penetrate and record additional returns at lower elevation. This was used to obtain a rough estimate of the crown base height needed to generate the trunk zone DEM. The approach used here was developed by Holmgren and Persson (2004) and has been applied by others (e.g. Kim et al. 2009). First, all the returns classified as vegetation were selected. Laser returns less than 2 m agl were

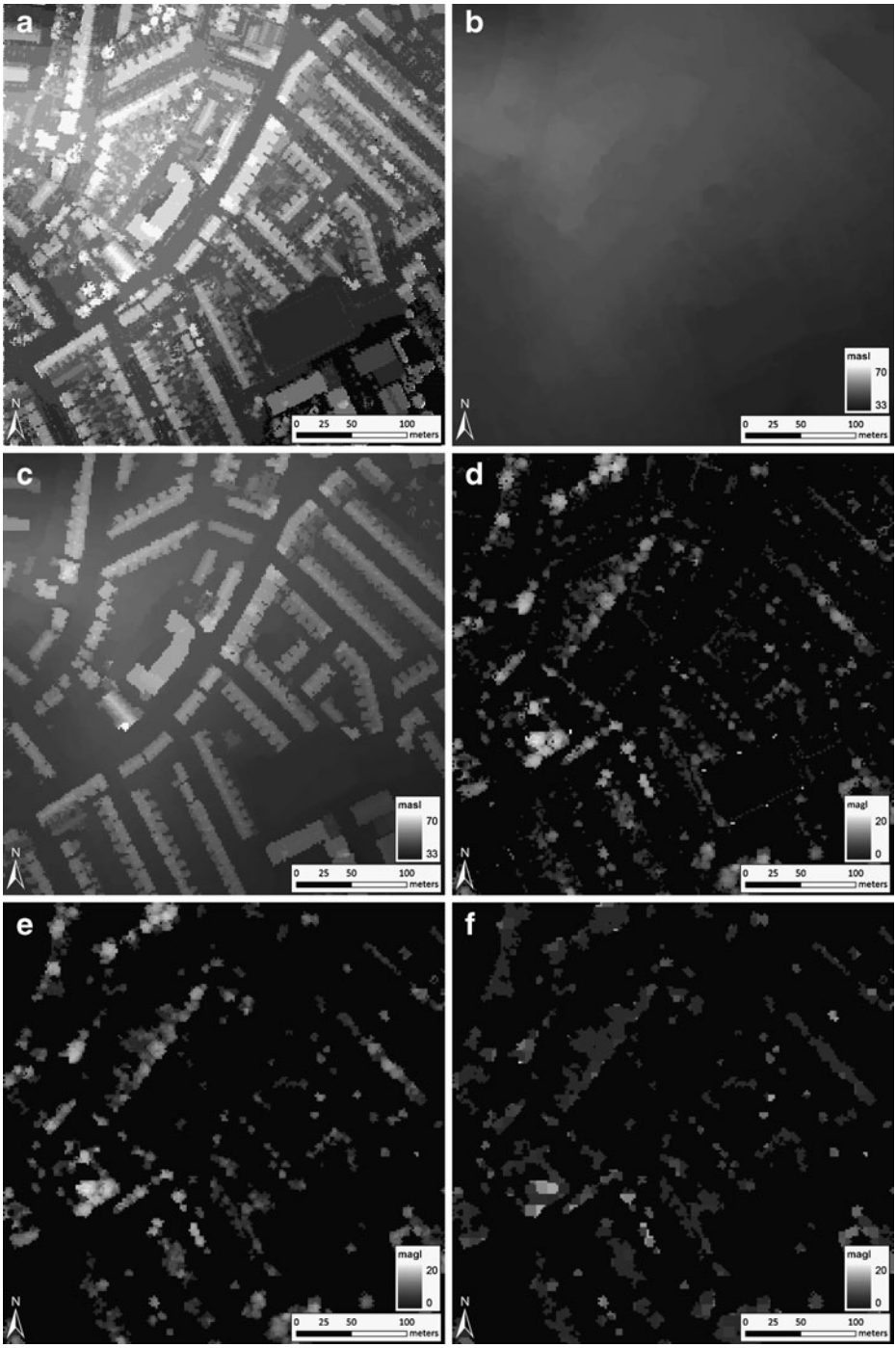

Fig. 2 Results generated in creating the digital elevation models (DEM) from LiDAR data (site 5N, see Fig. 1): **a** unprocessed LiDAR data, **b** ground DEM, **c** ground and building DEM, **d** canopy DEM before filtering, **e** canopy DEM after filtering, and **f** trunk zone DEM

omitted from the analysis to remove the effects of ground vegetation, cars and other obstacles found in the urban environment. The remaining laser points were classified as non-ground vegetation points. To estimate crown base height a 0.5-m interval was used. Each interval that contains ≤1% of the total number of non-ground laser points within an individual tree was set to zero and others to one. The crown base height was defined as the distance from ground to the lowest height layer where >1% of the data points were found. Holmgren and Persson (2004) used a segmentation process for separating different tree crowns and therefore could identify the returns that originated from a certain vegetation unit. As they had higher resolution laser data (0.44-m between laser hits on the ground) than this study, here vegetation laser returns were separated using a 10-m x 10-m grid for each study area. Within each grid cell a crown base height was estimated. Using this approach all vegetation pixels within a 10-m x 10-m grid have the same crown base height value. As an artefact of this, if a grid cell was located at the edge of vegetation, large overestimations may occur. After re-gridding the 10-m x 10-m grid to 2-m pixels this artefact was reduced by applying a 3 by 3 pixel median filter on single local maxima compared to the surrounding 8 pixels. If the crown base height and canopy height of a pixel were within 1 m, the crown base height was altered using a 3-by-3 pixel median filter. Very high crown base heights recorded from the processing (i.e., <15-m) are most likely related to large variations in canopy heights within each 10-m×10-m grid cell rather than actual crown base heights. These were classified as bush pixels. An example of a trunk zone DEM is shown in Fig. 2f.

The building and canopy DEMs for the 19 sites are shown in Fig. 3. In order to compare the sites, the building DEMs scale bars have a 45-m range except for 9S which is located on a relatively steep slope and therefore a higher range is used (60-m). Pixels with heights greater than the maximum height are shown as white pixels. All vegetation canopy DEMs have the same heights range (35-m) and pixels equal to 0 are transparent.

Spatial variability of urban morphology characteristics

Spatial variations of the various urban morphology characteristics influencing the urban climate and outdoor thermal comfort such as sky view factors, shadow patterns generated from buildings and vegetation characteristics are investigated using both the derived DEMs from the LiDAR data as well as from OS MasterMap® Topography Layer data. All sky view factors and shadow patterns derived used in this paper are calculated at surface level. LiDAR data also allows examination of the vertical distribution of the urban vegetation. The two types of vegetation DEMs (canopy and trunk zone) are used to derive vertical cross-sections for the 19 sites. The plan area densities were calculated each 0.5-m above the ground so that the vertical distribution of vegetation plan area cover could be derived. For each 0.5-m level above ground level a pixel by pixel comparison is made between the two vegetation DEMs so that the non-vegetation volume underneath the canopies is not accounted for. If a pixel value of the trunk zone DEM is higher than the height of the current 0.5-m section examined, this pixel is not included in the calculation of vegetation plan area. These cross sections with the vertical cross-sections of building plan areas give the total vertical distribution of all roughness elements found in the 19 sites.

SOLWEIG 2

SOLWEIG is a model that simulates spatial variations of 3D radiation fluxes and the mean radiant temperature (T_{mrt}) in complex urban settings. It is also able to model spatial variations of shadow patterns (Ratti and Richens 1999). T_{mrt} is one of the key meteorological variables

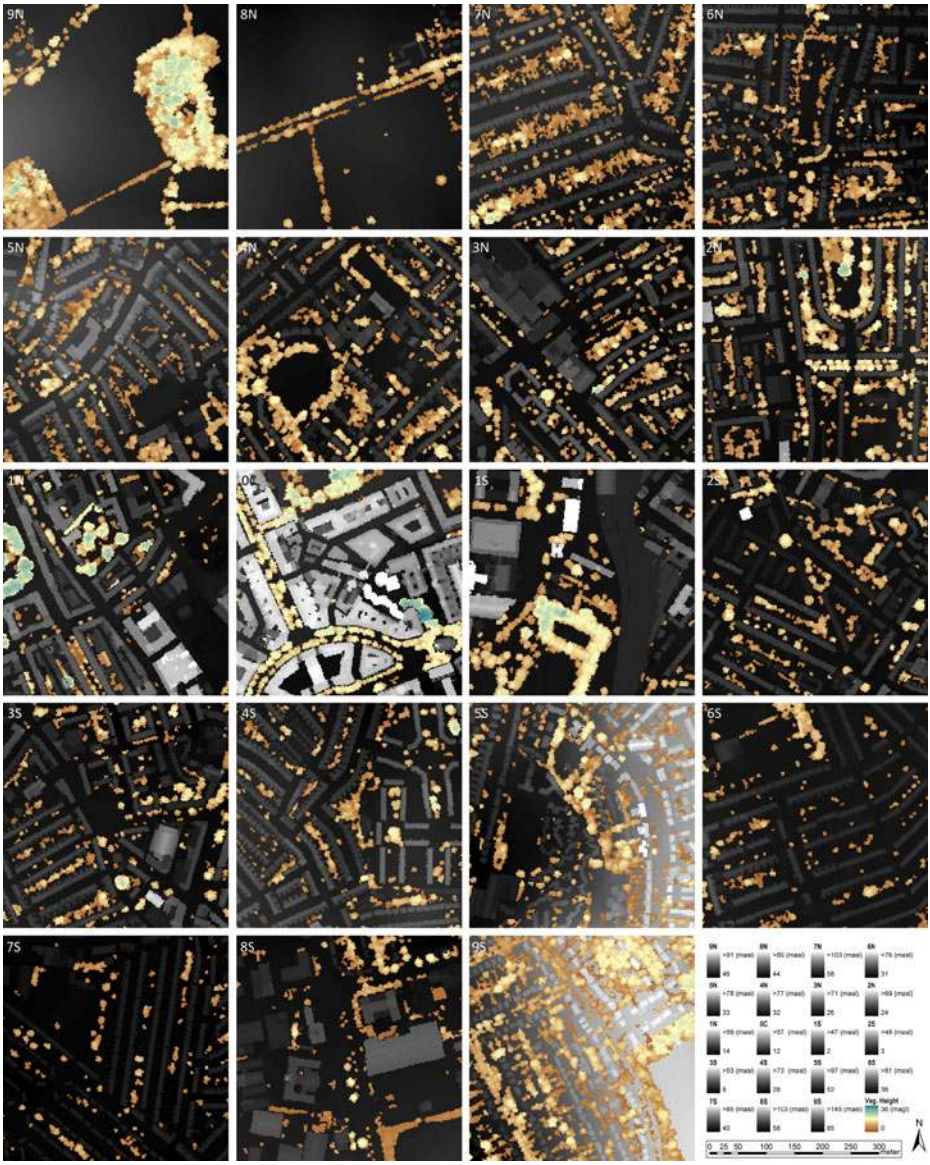

Fig. 3 Building DEMs overlaid by canopy DEMs derived from LiDAR data for the 19 sites (see Fig. 1)

governing human energy balance (e.g. Mayer et al. 2008) and the thermal comfort of people. It is derived from summing all shortwave and longwave radiation fluxes (both direct and reflected) to which the human body is exposed. In SOLWEIG, T_{mrt} is derived by modelling shortwave and longwave radiation fluxes in six directions (upward, downward and from the four cardinal points) and angular factors (Höppe 1992).

The model requires meteorological forcing data (global shortwave radiation ($K_{\downarrow}$), air temperature (T_a), relative humidity (RH)), urban geometry (high resolution urban DEMs), and geographic information (latitude, longitude and elevation). To determine $T_{mrt,}$

continuous maps of sky view factors (ψ) are required. The technique used to calculate ψ in SOLWIEG was originally developed by Ratti and Richens (1999) and further developed by Lindberg and Grimmond (2010). The evaluations of this method (e.g. Brown et al. 2001; Lindberg 2005 (Fig. 6), Lindberg and Grimmond 2010) have found that the results are very accurate. The results presented here use SOLWEIG 2.0 which is able to incorporate the presence and influence of vegetation (Lindberg and Grimmond 2011).

Application of SOLWEIG

For the surface morphology, the datasets derived from the LiDAR data are used as input to SOLWEIG. The meteorological forcing data are obtained from multiple sources. Global solar radiation ($K_{\downarrow}$) is obtained from a meteorological station located at the Strand Campus, King's College London (Fig. 1). To get near-surface T_a and humidity measurements, spatial averaged data from four local weather stations within the city centre of London are used (Learning Grid sites: Bow, Kensington, Westminster, Islington; http://weather.lgfl.org.uk). Here daytime situations are considered as this is when the beneficial effects of vegetation on outdoor heat stress through shading is likely to be, foremost because solar radiation and T_a will be high. Two clear days with high incoming shortwave radiation are examined (September 25th 2009, June 3rd 2010; referred to as autumn and summer day hereafter). In addition, these 2 days allow the impact of sun altitude on shadow patterns and T_{mrt} to be investigated.

The T_a range for the summer day was 11.3°C to 22.1°C and 11.7°C to 20.8°C for the autumn day. The midday variability in T_a between the Learning Grid sites was less than 1°C during both days. The maximum $K_{\downarrow}$ was 915 Wm^{-2} and 581 Wm^{-2} for the summer and autumn day, respectively. Both days are within the leaf-on period of the year. The forcing meteorological data are assumed to be the same for all 19 sites since only daytime periods are considered. A sensitivity analysis to the impact of air temperature and assumptions about diffuse radiation is performed.

Results and discussion

Vegetation and building characteristics in London

Various urban morphology characteristics for all 19 sites derived from the LiDAR dataset and OS MasterMap data are shown in Fig. 4. Clear local maxima of both mean building height (z_b) and building plan area density (λ_b) at the city centre are evident; the classical 'peak' where the strongest urban effect on the micro-climate usually is found (Oke 1987). This is also evident by visual examination of Fig. 3. Based on λ_b, the two northern most study areas located in Enfield (8N and 9N in Fig. 1) could be classified as rural (outside the 'cliff'), whereas the most southern study area (9S) is still within the urban environment. A clear 'plateau' with local maxima and minima is also evident in λ_b. At the local scale λ_b will influence the wind profile and roughness parameters (Grimmond and Oke 1999). Some very interesting patterns appear from the characteristics of vegetation (taller than 2.5 m) in the 19 sites. Similar to z_b there is a central peak in z_{v3}, meaning as building heights increases, vegetation height also increases. In the outskirts of the urban area there is taller vegetation; for example there is a forested area within 9N. When plotting z_b against z_{v3} a strong positive relation between the two is found (Fig. 5). The two vegetated/rural sites (8N and 9N) are plotted but excluded from the calculation of the linear trend. The reason for including the two rural data points in Fig. 5 is that they show the tendency of increasing

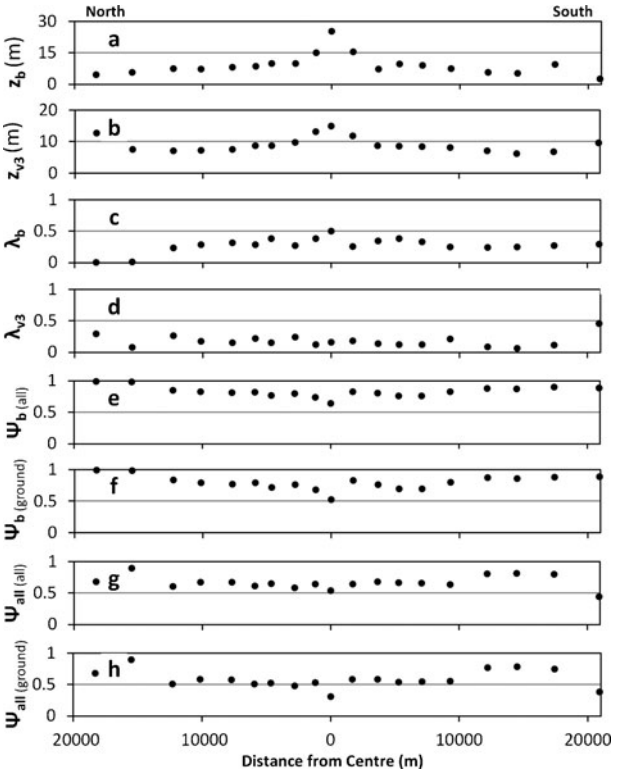

Fig. 4 Variations of morphological characteristics for a North-South transect through London (see Fig. 1): **a** mean building height (z_b), **b** mean vegetation height >2.5-m (z_{v3}), **c** plan area fraction of buildings (λ_b), **d** plan area fraction of vegetation >2.5-m (λ_{v3}), **e** sky view factor derived from building DEM (all pixels) ($\psi_{b(all)}$), **f** sky view factor derived from building DEM (ground level pixels) ($\psi_{b(ground)}$), **g** sky view factor from both building and vegetation DEMs (all pixels) ($\psi_{all(all)}$), and **h** sky view factor derived from both building and vegetation DEMs (ground level pixels) ($\psi_{all(ground)}$)

vegetation heights that could be found outside the urban environment and are located within the London boroughs. The maximum height of trees is naturally more limited than building heights which have higher peak values. Note that the LiDAR transect does not go over the tallest buildings of London (Fig. 1). The plan area density of vegetation λ_{v3} shows spots of larger amounts of vegetation i.e. parks and abundance of back gardens within certain areas of London. A tendency of increased λ_{v3} when reaching the outskirts of the urban area is also apparent. It should be noted that morphological parameters for vegetation (i.e. z_{v3} and λ_{v3}) only take vegetation taller than 2.5-m into account. If shorter vegetation, such as grass and small shrubs were included, the values of z_{v3} and λ_{v3} would change considerably especially at the outer sites. Potential for a bias to be introduced by not accounting for vegetation when determining urban roughness parameters is evident.

The peak found in z_b and λ_b is similarly found when examining the sky view factor derived from the building DEMs (ψ_b) (Lindberg and Grimmond 2010). ψ_b on all horizontal surfaces (i.e. roofs and ground) ($\psi_{b(all)}$) has similar values to ψ_b on the ground $\psi_{b(ground)}$ where $\psi_{b(all)}$ have higher values as elevated roofs are included. The largest discrepancies between these two parameters could be found when extensive building structures (e.g. industrial plants) are present within the area of interest. Values of $\psi_{b(ground)}$ also have a very similar pattern to λ_b with a strong negative correlation (R^2=0.83, not shown). The correlation between $\psi_{b(all)}$ and λ_b is even higher (R^2=0.86, not shown). When including the vegetation DEMs to create ψ from all essential 3D objects in the urban environment (ψ_{all}) (Lindberg and Grimmond 2011) the pattern changes to some extent compared to ψ_b with a

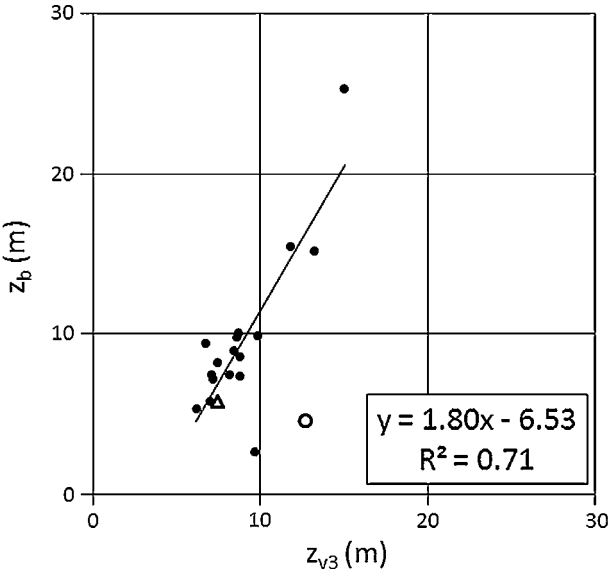

Fig. 5 Mean building height (z_b) versus mean vegetation height (z_{v3}). The trend line is based on urbanised sites (*black dots*, n=17). The triangle (predominately agricultural land) and the square (predominately forest) are the two 'rural' study areas within the Greater London Area (8N and 9N)

general reduction of ψ. The peak is still located in the city centre but large reductions of ψ are found at the outer sites where large amounts of vegetation are found. There is a positive correlation found between $\psi_{b(ground)}$ and $\psi_{all(ground)}$. However, the correlation is not very strong (R^2=0.48, not shown) indicating the importance of including vegetation when deriving continuous images of ψ in urban areas as argued by Chapman (2008).

Vertical cross sections of vegetation and buildings for the 19 sites are shown in Fig. 6. The distribution of the raw LiDAR returns/0.5-m section (Fig. 6a) is very similar to actual vertical distribution derived from the two vegetation DEMs (Fig. 6b). The two major differences are the plan area fraction at low levels. First, low level LiDAR returns are removed when generating the vegetation DEMs since these returns could include non-vegetation objects on the ground (e.g. vehicles, trash bins, humans etc.). Second, there seems to be a minor decrease of the plan area density from the vegetation DEMs compared to the raw LiDAR returns. The explanation for this is probably the distribution of LiDAR returns is higher within the centre of the canopy where the vegetation height also is high, whereas at the edges fewer and lower LiDAR returns are found. However, the pixel sizes of the DEMs are consistent (i.e. 2 m) and therefore appear to have lower mean heights that the actual LiDAR raw data (compare Figs. 4, 5, 6). The vertical distribution of vegetation (Fig. 6b) is in many ways similar to the vertical distribution of building structures (Fig. 6c) where plan area densities are shifted upward when moving closer to the city centre. Exceptions are found at the outskirts or outside the urban environment. Interesting patterns are also found in the very city centre (0C in Fig. 6a, b) where the plan area density of vegetation at low levels is very low indicative of the absence of near ground vegetation. This is probably because of the high level of maintenance required for vegetation in the dense central urban areas and the absence of residential gardens where low level vegetation is present typically. The big difference between the vertical distribution of buildings and vegetation is the increase found in vegetation at the outskirts of the city (also seen in Fig. 5). The implication of this is that the urban limit ('cliff') is erased when combining the vertical distribution of all 3D objects (Fig. 6d). Spots of low vegetation density are found at

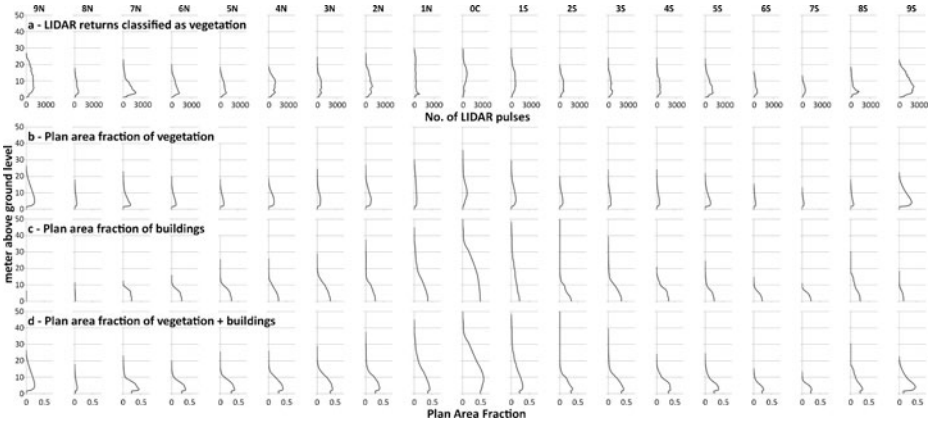

Fig. 6 Vertical distribution (in 0.5-m intervals) of buildings and vegetation of the 19 sites: **a** raw LiDAR returns classified as vegetation, **b** plan area density of vegetation, **c** plan area density of buildings, and **d** plan area density of buildings and vegetation

some more industrial sites (e.g. 6S and 7S). The vertical distribution of heights provides useful information for the calculation of frontal area index, which is frequently used in roughness parameter calculations (Grimmond and Oke 1999) and will be useful in some footprint calculations (Vesala et al. 2008).

Shadow patterns generated from buildings and vegetation

As noted in Section 1, one of the most important contributions of vegetation to thermal comfort during clear weather situations is the shade created by trees and bushes. Snapshots of shadow patterns from buildings (black) and vegetation (dark grey) for 0C at different times through 2 days are shown in Fig. 7. As expected, large differences are found when comparing the summer and autumn day, especially during early mornings and late evenings. The contribution of vegetation to the shadowing is relatively large, both during the autumn as well as on the summer day. In fact, vegetation seems to contribute more in summer than in autumn due to reduced building shadowing at ground level. This is examined later in this section. The boundary conditions of the model domain influence the shadow patterns, especially during early mornings and late evenings, as areas may be modelled as unshaded because the shadow would be cast by objects outside the model domain if present. This is seen clearly at 6 am (Fig. 7) where relatively large white areas are found at the eastern border of 0C. Also seen in Fig. 7, are the consequences of dense urban settings on solar access at ground level which would be exemplified for much of the year as shown by the shadow patterns during the autumn day.

To examine shadow patterns at ground level in more detail, shadows were modelled at 10-min intervals, as suggested by Yu et al. (2009) for complex urban environments, for the 19 sites for 2 days (Fig. 8). The difference between the shadow fractions from buildings with respect to the summer and autumn day is relatively similar for all sites, with a general decrease evident for the summer day due to higher sun altitude angles (Fig. 8a). The differences are largest at midday when the sun altitude angle is high. Some sites have larger differences between summer and autumn shadow fraction from buildings (e.g. 3N, 0C, 2S, and 3S). This could be related to building density represented by e.g. z_b, ψ_b etc. (Fig. 4).

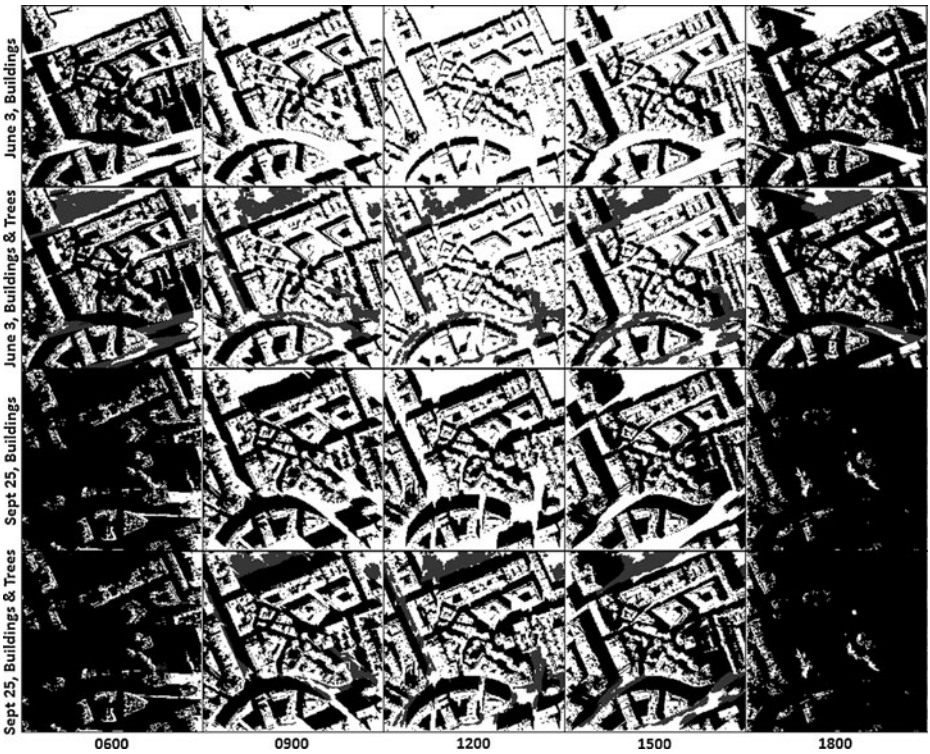

Fig. 7 Shadow patterns in study area 0C on the 3rd June 2010 and 25th September 2009 - at five times of day. Black areas are shadows generated from building whereas dark gray are shadows generated from vegetation

These large seasonal differences might also be related to specific configurations of the buildings within these study areas (Fig. 3).

Accounting for vegetation increases the total shadows on the ground (Fig. 8b). Comparing the general daily patterns of shadow fractions, with or without vegetation (Fig. 8a, b), indicates that shadows generated from buildings are the primary control on the amount of shade on the ground within the urban environment. However, the more vegetation present, the more likely that there is an increase in the amount of shaded ground (e.g. 9N and 9S).

Daytime mean shadow fractions on the ground are shown in Fig. 9. These are calculated from 10-m in shadow images, while the sun is above the horizon (N=96 and N=71 for the

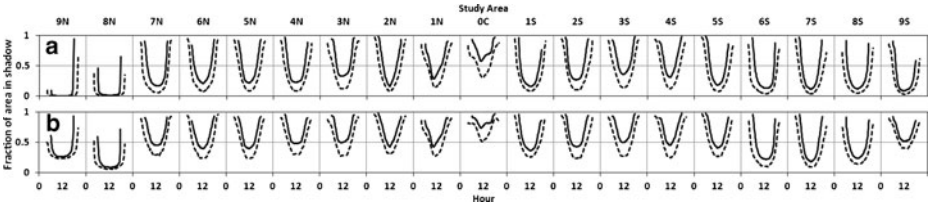

Fig. 8 Daytime variations of shadow fraction at ground level for the 19 sites on 3rd June (*dashed*) and 25th September (*solid*): **a** shadow fractions from buildings, and **b** from both buildings and vegetation

summer and autumn day, respectively). The latitude is considered the same for all sites. The graphs of transects (Fig. 9) reveal a number of interesting features regarding shadows present in a city such as London. The shadow fractions from buildings at ground level follow, as expected, the pattern where the autumn day has higher fractions than the summer day due to lower sun altitude angles. The correlation between plan area fractions (λ), sky view factors (ψ) and shadow fractions are shown in Fig. 10. An almost perfect fit is obtained between shadow fractions and $\psi_{b(ground)}$ derived from the building DEM (Fig. 10b) using a second polynomial trend line (summer: R^2=0.99, autumn: R^2=0.99) but λ_b also (Fig. 10a) show very high correlations with shadow fraction using a linear trend (summer: R^2=0.85, autumn: R^2=0.87). z_b is poorly correlated (not shown) with shadow fractions (summer: R^2=0.44, autumn: R^2=0.42); even a simple 'distance from centre' measure (not shown) has a higher correlation than z_b (summer: R^2=0.66, autumn: R^2= 0.62). Including vegetation increases the scattering and decreases the correlation between λ, ψ and shadow fractions. This is because 3D vegetation have varying trunk zone heights which are not represented in the 2D plan area densities. Although trunk zone heights are included in $\psi_{all(ground)}$, the correlation decreases because of the dominance of building shadowing within the urban environment (i.e. vegetation shadow patterns that would have been on the ground are overshadowed by building shadows).

As noted, the vegetation shadow fraction for 0C was greater for summer than the autumn day (Fig. 7). This site (0C, Fig. 9) is the only one where the shadow fraction significantly increases during the summer day compared to the autumn day. This is probably because shadowing from buildings in the autumn blocks out the shadows from vegetation whereas in summertime the sun light reaches the canyon floor due to high sun altitude angle and vegetation shadow now become visible. This is probably the combination of the tall building heights and dense urban structures. This finding exemplifies the importance of vegetation within dense urban structure and how heat stress could be reduced by the use of vegetation shadowing during the summer months, when heat wave events are most likely to occur in the part of the city where urban heat stress is likely to be the greatest. At high sun altitude angles the majority of the shadow from a vegetation canopy will be located within the radius of the canopy i.e. underneath the canopy. This implies that the increase in vegetation shadow at high sun altitude angles would not have been spotted if vegetation would have been treated as 2.5D objects (e.g. Yu et al. 2009). However, the new shadowing technique using trunk zone DEMs (Lindberg and Grimmond 2011) reveals this.

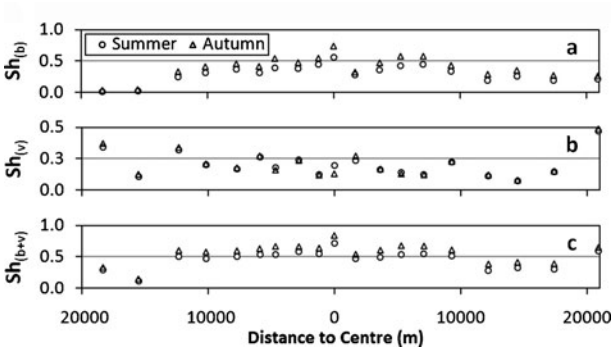

Fig. 9 Fraction of area covered with shadow at ground level for each siteintegrated at 10-m in intervals over daytime period on June 3rd and 25th September for a North-South transect **a** for buildings ($Sh_{(b)}$), **b** for vegetation ($Sh_{(V)}$) and **c** combined ($Sh_{(b,v)}$)

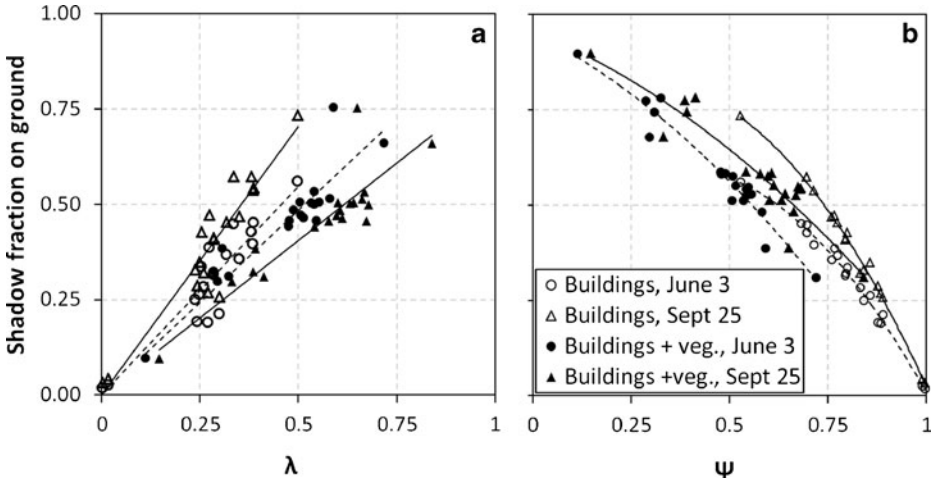

Fig. 10 Shadow fractions on ground versus **a** plan area fraction (λ) and **b** sky view factor (ψ). Solid trend lines are used for autumn situations and dashed trend lines are used for summer situations

The influence of vegetation and building morphology on T_{mrt}

When SOLWEIG 2.0 (Lindberg and Grimmond 2011) is used to calculate the average daytime T_{mrt}, the lowest values are found in the city centre both when vegetation is accounted for and not (Fig. 11a, b). The overall pattern for the 19 sites is very similar to both ψ (Fig. 4) and shadow patterns (Fig. 7). When the vegetation scheme is used T_{mrt} is reduced, with the largest effect in areas with a high fraction of vegetation (λ_{v3}), both for summer and autumn. There is a very high correlation between the difference in T_{mrt} using the vegetation scheme or not and λ_{v3} (summer: R^2=0.96, autumn: R^2=0.91) indicating that λ_{v3} could be used as a measure for heat stress mitigation using vegetation. The mean reduction along the transectin T_{mrt} when vegetation is accounted for is 3.1°C (min 1.4 (7S) max 7.5 (9S)) during the summer and 3.2°C (min 1.2 (7S) max 3.5 (9S)) during autumn.

The results of a sensitivity test to increasing the T_a forcing data by 2°C on the summer day (keeping the vapour pressure constant) produces a mean increase in T_{mrt} of 1.6°C for both vegetated and non-vegetated cases. When a much greater increase in T_a of 10°C is used, which may be more likely under a heat wave situation, the increase in T_{mrt} for vegetated simulations was 7.9°C and 8.5°C for non-vegetated conditions.

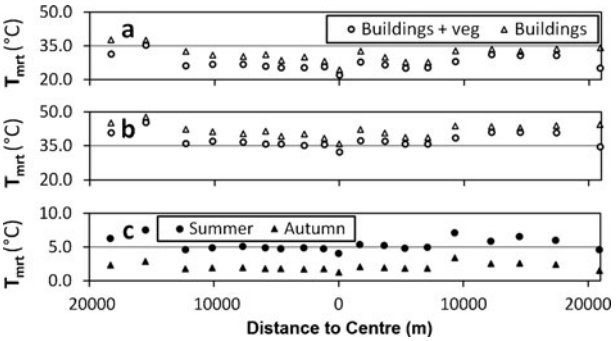

Fig. 11 Average daytime values of $T_{mrt\ (standing\ person)}$(°C) at ground level for a North-South transect through London. **a** 25th September 2009. **b** 3rd June 2010. **c** Difference in $T_{mrt\ (standing\ person)}$(°C) (buildings+veg.) on the 3rd June 2010 between original values of estimated diffuse radiation (D) and with a 25% reduction of D

In this case the diffuse shortwave radiation (D) is unknown so it is modelled within SOLWEIG using $K_{\downarrow}$, T_a, *RH* and sun altitude (Reindl et al. 1990). The $D/K_{\downarrow}$ratio is estimated to be 0.2 at noon on the clear summer day (3 June 2010) which is probably an overestimate that will affect the results. Analysis of data for the same summer day for a rural site (Wallingford) run by the Centre for Ecology & Hydrology (CEH) approximately 70 km west had a $D/K_{\downarrow}$ ratio of 0.1. In urban areas one assumes a larger $D/K_{\downarrow}$ due to increased scattering (e.g. Lalas et al. 1987; Robaa 2006). The impact of reducing the modelled D by 25% (i.e. $D/K_{\downarrow}=0.15$) the spatial patterns along the transect are maintained (not shown) and results in an overall reduction to T_{mrt} (2°C—autumn; 5°C—summer day, Fig. 11e). The difference is most pronounced at the low-density sites (i.e. low ψ and high λ_b) as a higher proportion of diffuse radiation is able to reach ground level without being blocked by obstacles such as buildings and trees (Fig. 11e). The model is sensitive to D, but the overall pattern and the reduction of T_{mrt} when vegetation is considered, are maintained by SOLWEIG.

SOLWEIG can simulate spatial variations of 3D radiation fluxes and mean radiant temperature. The spatial variations of T_{mrt} for 0C (3 June 2010 3 pm) with D reduced by 25% are shown in Fig. 12a. The highest T_{mrt} values are in the narrow street canyons and in sunlit areas underneath the vegetation canopy. This is because of the hemispheric blocking of the relatively cooler sky by buildings and trees. Human thermal comfort is correlated to T_{mrt} (e.g. Matzarakis et al. 2010) but convective cooling is not accounted for in T_{mrt}. Underneath the vegetation canopy the wind speed is likely to be reduced, especially at locations that are close to building walls or situated in very dense urban environments. Thus, thermal indices such as Physiological Equivalent Temperature (PET) (Mayer and Höppe 1987) may be higher at such locations. Lower T_{mrt} values are found in shadowed areas, with the lowest values in shadowed locations at roof level. The sensitivity of T_{mrt} to D (original minus D* 0.25) can be seen in the difference map (Fig. 12b). As expected, areas with low ψ have reduced T_{mrt} when D is reduced. The opposite is also evident. Even though the differences are small this demonstrates the preference for observed D values where possible and the need to consider alternative methods to calculate D in future versions of SOLWEIG.

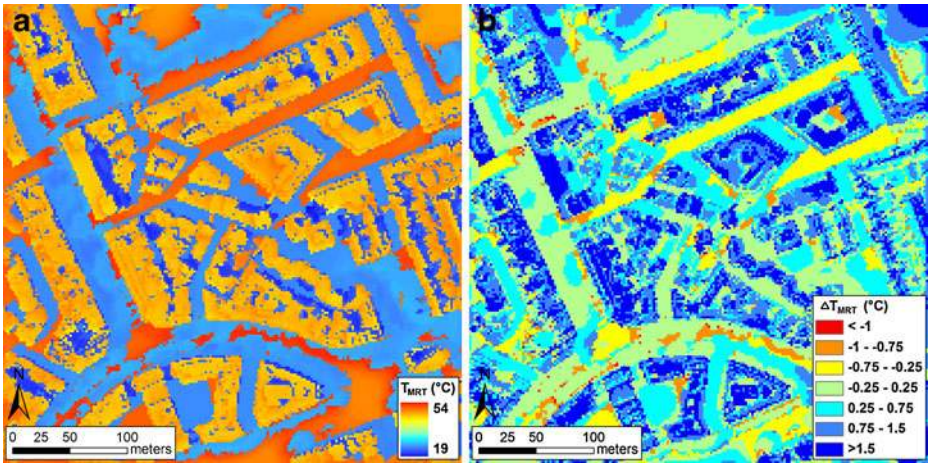

Fig. 12 **a** Spatial variations of$T_{mrt\ (standing\ person)}$(°C) for 0C 3 pm 3 June (D reduced by 25%). **b** Difference map between $T_{mrt\ (standing\ person)}$(°C) estimated with original modelled diffuse radiation and reduced (25%) modelled diffuse radiation

Conclusions

LiDAR data with the SOLWEIG model are used to examine the variability of urban morphology, shadow patterns and T_{mrt} across London. The following conclusions are drawn about the urban morphology for this European megacity, likely they apply to many other urban areas:

- Clear local maxima of both mean building height (z_b) and building plan area density (λ_b) in the city centre are evident.
- The tallest vegetation is in the city centre.
- There is a strong positive relation building height and vegetation height.
- The plan area density of vegetation (λ_{v3}) has an overall tendency to increase towards the outskirts of the urban area. This increase is associated with parks and abundance of residential back gardens.
- There is a minima in sky view factor in the city centre derived from the building DEMs (ψ_b).
- There is high overall correlation between z_b, λ_b and ψ_b
- Accounting for vegetation in ψ as part of the 3D objects in the urban environment (ψ_{all}) results in a general reduction of ψ compared to ψ_b. The peak remains in the city centre but with large reductions in ψ found in the outer areas of the city where large amounts of vegetation are found. There is a positive correlation found between $\psi_{b(ground)}$ and $\psi_{all(ground)}$. However, the correlation is not very strong indicating the importance of including vegetation when deriving continuous images of ψ in urban areas.

The following conclusions are drawn based on examining the shadow patterns and T_{mrt} results from modelling 2 days (one autumn and one summer) with SOLWEIG:

- Shadow fractions from buildings at ground level follow the expected higher values on the autumn day than the summer day due to the lower sun altitude angles.
- Correlations between plan area fractions (λ), sky view factors (ψ) and shadow fractions are very high suggesting that ψ could be used to estimate shadow fractions in urban environments.
- Contribution of vegetation to shadowing at ground level is greater during summer than in autumn. This highlights that vegetation is an effective method to reduce heat stress within dense urban structures during heat wave events.
- Daytime average T_{mrt} is lowest in the densest urban environments due to shadowing foremost from buildings but also trees.
- It is shown clearly that vegetation could be used to reduce T_{mrt} within the urban environment. The average reduction in T_{mrt} was 3.1°C for summer and 3.2°C for autumn.
- A very strong correlation between λ_{v3} and reduction in T_{mrt} is found.

The results presented highlight the potential for a number of climate sensitive planning opportunities in urban areas at the local scale (i.e. 10^2-5×10^3 m). Increasing the amount of vegetation, in all kinds of urban settings, has the potential to be an effective method to mitigate enhanced heat wave episodes. Having knowledge of the vegetation distribution in urban areas is beneficial in understanding for a wide number of processes (e.g. hydrology, climatology, ecology, physiology); for example, 3D morphology has utility in wind related applications such as deriving roughness parameters from all obstacles in the urban environment (i.e. both buildings and vegetation). In this study the impact of (not) accounting for the presence of vegetation is considered with respect to mean radiant

temperature (T_{mrt}). This variable provides an indication of the thermal stress that is likely to be encountered by people outdoors. Given that in many urban areas planting trees is being advocated, it is beneficial to determine the morphology of the current trees and the impact of accounting for their presence.

Acknowledgements This work is supported by FORMAS—the Swedish Research Council for Environment, Agricultural Sciences and Spatial Planning, European Community's Seventh Framework Programme FP/2007–2011 BRIDGE (211345), NERC Airborne Remote Sensing Facility (GB08/19), the Centre for Ecology & Hydrology (CEH) and King's College London (in particular all those who contribute to the urban micrometeorology group).

References

Akbari H (2002) Shade trees reduce building energy use and CO2 emissions from power plants. Environ Pollut 116:S119–S126

Akbari H, Pomerantz M, Taha H (2001) Cool surfaces and shade trees to reduce energy use and improve air quality in urban areas. Sol Energy 70:295–310

Ali-Toudert F, Mayer H (2006) Numerical study on the effects of aspect ratio and orientation of an urban street canyon on outdoor thermal comfort in hot and dry climate. Build Environ 41:94–108

Ali-Toudert F, Mayer H (2007a) Effects of asymmetry, galleries, overhanging façades and vegetation on thermal comfort in urban street canyons. Sol Energy 81:742–754

Ali-Toudert F, Mayer H (2007b) Numerical study on the effects of aspect ratio and orientation of an urban street canyon on outdoor thermal comfort in hot and dry climate. Build Environ 42:1553–1554

Bergen KM, Goetz SJ, Dubayah RO, Henebry GM, Hunsaker CT, Imhoff ML, Nelson RF, Parker GG, Radeloff VC (2009) Remote sensing of vegetation 3D structure for biodiversity and habitat: review and implications for lidar and radar spaceborne missions. J Geophys Res 114:G00E06

Brown MJ, Grimmond CSB, Ratti CF (2001) Comparison of methodologies for computing sky view factor in urban environments. In International Society of Environmental Hydraulics Conference, Tempe, AZ, December 2001, LA-UR-01-4107

Ca VT, Asaeda T, Abu EM (1998) Reductions in air conditioning energy caused by a nearby park. Energy Build 29:83–92

Chapman L (2008) An introduction to 'upside–down' remote sensing. Prog Phys Geogr 32:529–542

Goodwin NR, Coops NC, Tooke TR, Christen A, Voogt JA (2009) Characterizing urban surface cover and structure with airborne lidar technology. Can J Remote Sens 35:297–309

Grimmond CSB, Oke TR (1991) An evaporation-interception model for urban areas. Water Resour Res 27:1739–1755

Grimmond CSB, Oke TR (1999) Aerodynamic properties of urban areas derived, from analysis of surface form. J Appl Meterol 38:1262–1292

Heisler GM (1990) Mean wind speed below building height in residential neighborhoods with different tree densities. ASHRAE Transactions 96:1389–1396

Hirano Y, Yasuoka Y, Ichinose T (2004) Urban climate simulation by incorporating satellite-derived vegetation cover distribution into a mesoscale meteorological model. Theor Appl Climatol 79:175–184

Holmgren J, Persson Å (2004) Identifying species of individual trees using airborne laser scanner. Remote Sens Environ 90:415–423

Honjo T, Takakura T (1990–1991) Simulation of thermal effects of urban green areas on their surrounding areas. Energy Build 15:443–446

Höppe P (1992) A new procedure to determine the mean radiant temperature outdoors. Wetter und Leben 44:147–151

IPCC (2007) AR4 Synthesis report, full report, intergovernmental panel on climate change, http://www.ipcc.ch/pdf/assessment-report/ar4/syr/ar4_syr.pdf

Kim S, McGaughey RJ, Andersen H-E, Schreuder G (2009) Tree species differentiation using intensity data derived from leaf-on and leaf-off airborne laser scanner data. Remote Sens Environ 113:1575–1586

Lalas DP, Petrakis M, Papadopoulos C (1987) Correlations for the estimation of the diffuse radiation component in Greece. Sol Energy 39:455–458

Lin T-P, Matzarakis A, Hwand R-L (2010) Shading effect on long-term outdoor thermal comfort. Build Environ 45:213–211
Lindberg F (2005) Towards the use of local governmental 3-D data within urban climatology studies. Mapping and Image Science 2005(2):4–9
Lindberg F, Grimmond CSB (2010) Continuous sky view factor maps from high resolution urban digital elevation models. Climate Research 42:177–183
Lindberg F, Grimmond CSB (2011) The influence of vegetation and building morphology on shadow patterns and mean radiant temperatures in urban areas: model development and evaluation. Theoretical and Applied Climatology doi:10.1007/s00704-010-0382-8
Lindberg F, Holmer B, Thorsson S (2008) SOLWEIG 1.0—modelling spatial variations of 3D radiant fluxes and mean radiant temperature in complex urban settings. Int J Biometeorol 52:697–713
Masmoudi S, Mazouz S (2004) Relation of geometry, vegetation and thermal comfort around buildings in urban settings, the case of hot arid regions. Energy Build 36:710–719
Matzarakis A, Endler C (2010) Adaptation of thermal bioclimate under climate change conditions—the example of physiologically equivalent temperature in Freiburg, Germany. Int J Biometeorol 54:479–483
Matzarakis A, Mayer H, Iziomon MG (1999) Applications of a universal thermal index: physiological equivalent temperature. Int J Biometeorol 43:76–84
Matzarakis A, Rutz F, Mayer H (2010) Modelling radiation fluxes in simple and complex environments: basics of the RayMan model. Int J Biometeorol 54:131–139
Mayer H, Hoslt J, Dostal P, Imbery F, Schindler D (2008) Human thermal comfort in summer within an urban street canyon in Central Europe. Meteorologische Zeitschrift 17(3):241–250
Mayer H, Höppe P (1987) Thermal comfort of man in different urban environments. Theor Appl Climatol 38:43–49
McCarthy MP, Best MJ, Betts RA (2010) Climate change in cities due to global warming and urban effects. Geophys Res Lett 37:L09705
McGaughey RJ (2009) FUSION/LDV: Software for LiDAR data analysis and visualization. United States Department of Agriculture, Seattle
Meehl GA, Tebaldi C (2004) More Intense, more frequent, and longer lasting heat waves in the 21st century. Science 305:994–997
Næsset E (2004) Accuracy of forest inventory using airborne laser scanning: evaluating the first nordic full-scale operational project. Scand J For Res 19:554–557
Oke TR (1987) Boundary layer climates. Routledge, Cambridge, p 435
Ordnance Survey (2010) © Crown database right 2010. An Ordnance Survey/EDINA supplied service. Assessed 2009-10-13. http://www.ordnancesurvey.co.uk/oswebsite/
Pascal M, Laaidi K, Ledrans M, Baffert E, Caserio-Schönemann C, Le Tertre A, Manach J, Medina S, Rudant J, Empereur-Bissonnet P (2006) France's heat health watch warning system. Int J Biometeorol 50:144–153
Picot X (2004) Thermal comfort in urban spaces: impact of vegetation growth—case study: Piazza dellaScienza, Milan, Italy. Energy Build 36:329–334
Ratti CF, Richens P (1999) Urban texture analysis with image processing techniques. Proc CAADFutures99. Atlanta, GA
Reindl DT, Beckman WA, Duffie JA (1990) Diffuse fraction correlation. Sol Energy 45:1–7
Robaa SM (2006) A study of solar radiation climate at Cairo urban area, Egypt and its environs. Int J Climatol 26:1913–1928
Robitu M, Musy M, Inard C, Groleau D (2006) Modeling the influence of vegetation and water pond on urban microclimate. Sol Energy 80:435–447
Shashua-Bar L, Pearlmutter D, Erell E (2010) The influence of trees and grass on outdoor thermal comfort in a hot-arid environment. Int J Climatol doi:10.1002/joc.2177
Simpson JR (2002) Improved estimates of tree-shade effects on residential energy use. Energy Build 34:1067–1076
Upmanis H, Eliasson I, Lindqvist S (1998) The influence of green areas on nocturnal temperatures in a high latitude city (Goteborg, Sweden). Int J Climatol 18:681–700
Vesala T, Kljun N, Rannik Ü, Rinne J, Sogachev A, Markkanen T, Sabelfeld K, Foken TH, Leclerc MY (2008) Flux and concentration footprint modelling: state of the art. Environ Pollut 152:653–666
WHO/WMO/UNEP (1996) Climate and health: the potential impacts of climate change. Swizterland, Geneva
Yu B, Liu H, Wu J, Lin W-M (2009) Investigating impacts of urban morphology on spatio-temporal variations of solar radiation with airborne LiDAR data and a solar flux model: a case study of downtown Houston. Int J Remote Sens 30:4359–4385